Self-consistency over the charge-density in dynamical mean-field theory: a linear muffin-tin implementation and some physical implications.

L. V. Pourovskii[1], B. Amadon[2], S. Biermann[1], and A. Georges[1]

[1] *Centre de Physique Théorique, Ecole Polytechnique, CNRS, 91128 Palaiseau Cedex, France*
[2] *Département de Physique Théorique et Appliquèe,*
CEA, B.P. 12, 91680 Bruyères-le-Châtel, France
(Dated: February 1, 2008)

We present a simple implementation of the dynamical mean-field theory approach to the electronic structure of strongly correlated materials. This implementation achieves full self-consistency over the charge density, taking into account correlation-induced changes to the total charge density and effective Kohn-Sham Hamiltonian. A linear muffin-tin orbital basis-set is used, and the charge density is computed from moments of the many body momentum-distribution matrix. The calculation of the total energy is also considered, with a proper treatment of high-frequency tails of the Green's function and self-energy. The method is illustrated on two materials with well-localized $4f$ electrons, insulating cerium sesquioxide Ce_2O_3 and the γ-phase of metallic cerium, using the Hubbard-I approximation to the dynamical mean-field self-energy. The momentum-integrated spectral function and momentum-resolved dispersion of the Hubbard bands are calculated, as well as the volume-dependence of the total energy. We show that full self-consistency over the charge density, taking into account its modification by strong correlations, can be important for the computation of both thermodynamical and spectral properties, particularly in the case of the oxide material.

I. INTRODUCTION

While density functional theory (DFT)[1,2] in conjunction with the local density approximation (LDA) is remarkably successful in predicting ground-state properties of a wide range of real materials, it has been found unable to provide the correct description of so-called strongly correlated materials (transition metal oxides, many actinide and lanthanide-based materials, high T_c superconductors) even on a qualitative level. In order to overcome these shortcomings of the traditional DFT-LDA scheme, a combination of the DFT-based band structure techniques with dynamical mean-field theory (DMFT)[3] has been proposed[4,5,6]. In DMFT one introduces a strong local Coulomb interaction acting between electrons of a correlated band (for example, the $d-$band in transition- metal oxides or the $f-$band in actinides). The self-energy is found by first mapping a full solid onto a quantum impurity model involving a single atom hybridized with an effective bath, and solving this effective model using many-body techniques. This self-energy is then promoted to all lattice sites, therefore restoring the translational invariance of the crystal. As a result one obtains the fully interacting Green's function for the system, from which a wide range of properties can be extracted.

Starting from the end of the 90's, this new LDA+DMFT approach to the electronic structure of strongly correlated materials has been rapidly developing, and a number of different implementations have been proposed and applied to calculations of the spectral and, in some cases, thermodynamic properties, of Mott insulators, ferromagnetic 3-d metals, Ce, Pu, and other actinide systems (for reviews, see[7,8,9]). Up to date most LDA+DMFT calculations have been performed using a partially self-consistent scheme, where the local self-energy is obtained from a DMFT calculation with the *fixed* LDA charge density, and, hence, with a *fixed* LDA Hamiltonian. Therefore, in this simplified scheme one neglects the impact of the strong on-site Coulomb interaction on the charge distribution.

Implementing full self-consistency over the charge density is a somewhat delicate task. Several fully self-consistent LDA+DMFT schemes have been discussed in the literature[10,11,12,13], while only two actual implementations have appeared up to date. The first one, due to Savrasov and Kotliar[10], is based on the full-potential LMTO method. In order to compute the LDA+DMFT charge density one has to construct from the LDA Hamiltonian and the DMFT local self-energy a local Green's function of the interacting system. In Ref. [10] this task has been accomplished by first finding the (right- and left-) eigenfunctions and eigenvectors of the Kohn-Sham Hamiltonian combined with the self-energy $H_{KS}(\mathbf{k}) + \Sigma(i\omega)$ and then performing the Brillouin zone integration by means of the tetrahedron method[14]. As the self-energy is a complex function, this scheme requires the diagonalization of a non-Hermitian matrix for each $\mathbf{k}-$point and Matsubara frequency, which is a computationally demanding task. Another scheme has been proposed by Minar *et al.*[11] on the basis of the KKR Green's function method. Their approach requires solving the radial Dirac equation with the self-energy being added to the LDA atomic potential. Generally the self-energy is a non-diagonal matrix, therefore an additional coupling is generated between Dirac equations for different magnetic quantum numbers m, making the solution of the Dirac equation a highly non-trivial task. Minar *et al.* applied their scheme to calculations of the FeNi binary alloy, which forms a cubic lattice. Hence, in this case, both the Green's function and self-energy are diagonal in the orbital indexes, and there is no additional coupling generated in the Dirac equation. However, this problem will certainly arise for lower symmetry lattices or $f-$electron compounds.

In the present article, we propose and apply a relatively simple implementation of the fully self-consistent LDA+DMFT method. The charge density (including correlation effects described by the many-body self-energy) is expressed in terms of a $\mathbf{k}$-dependent momentum-distribution matrix $N_{LL'}^{\mathbf{k}}$, which is obtained from the many-body Green's function by summing over frequency. Furthermore, using a linear muffin-tin orbital basis set, we reduce the calculation of the charge density to that of three moments, involving this matrix and the Kohn-Sham Hamiltonian itself. In order to calculate the total energy, a functional of both the charge density and the on-site components of the Green's function associated with local orbitals can be used[7,10], as previously discussed by Savrasov and Kotliar. In all these calculations, obtaining the charge density and total energy with sufficient accuracy requires a careful treatment of the high-frequency tails of the Green's function and self-energy, and we derive here appropriate formulas to handle this issue.

In order to illustrate this approach, and to assess the importance of full self-consistency on the charge density, we perform in this article fully-selfconsistent LDA+DMFT calculations of the density of states, the band structure, and the volume-dependence of the total energy of two materials: γ-cerium and cerium sesquioxide Ce_2O_3. The quasi-localized f-electrons are treated using DMFT in conjunction with the Hubbard-I approximation as a quantum impurity solver[15]. Our theory reproduces the experimentally observed splitting of the rare-earth f-band into occupied lower and empty upper Hubbard bands, while the conventional LDA calculations incorrectly predict this band to be pinned at the Fermi level[16]. We show that the self-consistency over the charge density shifts significantly the positions of the Hubbard bands (in comparison to using a

frozen LDA charge density), in both γ-Ce and Ce_2O_3. It is therefore important for the correct description of spectral and optical properties of those materials.

The paper is organized as follows. In Section II, we describe our self-consistent LDA+DMFT implementation. After a brief reminder of the basic LDA+DMFT scheme (Sec. II A) and of the LMTO basis-set (Sec. II B), we derive the expression for the charge density in this basis (Sec. II C). After reviewing the total energy functional of LDA+DMFT (Sec. II D), we discuss the practical calculation of the energy (Sec. II E). We conclude Sec. II by describing the specific form of the interaction vertex used in this article, as well as the double counting correction and the Hubbard-I impurity solver (Sec. II F). Section III presents the results for Ce_2O_3 (Sec. III A) and γ-Ce (Sec. III B).

II. IMPLEMENTATION OF THE FULLY SELF-CONSISTENT LDA+DMFT METHOD

A. The LDA+DMFT formalism: a brief reminder

The LDA+DMFT approach to electronic structure is based on two key quantities: the charge density $\rho(\mathbf{r})$ and the local Green's function of the solid, or more precisely the projection $G_{ab}(\omega)$ of the full Green's function onto a single atomic site and on the subspace of correlated orbitals. Both quantities have to be determined self-consistently, following an iterative cycle which is summarized on Fig. 1. This can be rationalized as a functional of both $\rho(\mathbf{r})$ and G_{ab}, as detailed later in Sec. II D.

Let us follow this iterative cycle, starting from a charge density profile $\rho(\mathbf{r})$. A Kohn-Sham (KS) potential is constructed from $\rho(\mathbf{r})$ as:

$$v_{KS}(\mathbf{r}) = v_c(\mathbf{r}) + v_H\left[\rho(\mathbf{r})\right] + v_{xc}\left[\rho(\mathbf{r})\right] \tag{1}$$

in which v_c is the periodic potential of the (fixed) ions, $v_H = \int d\mathbf{r}' \frac{e^2}{|\mathbf{r}-\mathbf{r}'|}\rho(\mathbf{r}')$ is the Hartree potential, and $v_{xc} = \delta E_{xc}/\delta\rho(\mathbf{r})$ is the exchange-correlation potential. Hence, the functional dependence of v_{KS} on $\rho(\mathbf{r})$ is kept identical to that of conventional DFT. In practice, v_{xc} will be computed from $\rho(\mathbf{r})$ using the LDA form of the exchange-correlation energy $E_{xc}^{LDA} = \int d\mathbf{r}\rho(\mathbf{r})\varepsilon[\rho(\mathbf{r})]$, with $\epsilon[\rho]$ the energy density of the homogeneous electron gas. Solving the single-particle Schrödinger equation associated with v_{KS} yields the KS eigenenergies $\epsilon_{\mathbf{k}\nu}^{KS}$ and eigenfunctions $|\mathbf{k}\nu\rangle$ (with ν a band index), forming the KS effective one-particle hamiltonian:

$$H_{KS} = \sum_{\mathbf{k}\nu} \epsilon_{\mathbf{k}\nu}^{KS} |\mathbf{k}\nu\rangle\langle\mathbf{k}\nu| \tag{2}$$

At this stage, it is convenient to introduce a set of localized basis functions $\chi_{L\mathbf{R}}(\mathbf{r})$, where $\mathbf{R}$ denotes an atomic position, and L stands for all orbital indices (e.g., $L = \{l, m, \sigma\}$). In the following, we shall consider linearized muffin-tin orbitals (LMTOs), but different basis-sets can be used and have been considered in the literature[12,17,18] (e.g., Wannier functions). The electron creation operator at a point $\mathbf{r}$ in the solid can be expanded on this basis as:

$$\psi^\dagger(\mathbf{r}) = \sum_{\mathbf{R},L} \chi_{L\mathbf{R}}^*(\mathbf{r})\, c_{L\mathbf{R}}^\dagger \tag{3}$$

and the KS hamiltonian reads:

$$H_{KS} = \sum_{\mathbf{k}L} H_{LL'}^{KS}(\mathbf{k}) c_{\mathbf{k}L}^\dagger c_{\mathbf{k}L'} \tag{4}$$

In the LDA+DMFT approach, this Hamiltonian is supplemented by many-body terms. These many-body terms act in the subspace generated by a set of orbitals corresponding in practice to the orbitals (e.g d or f-orbitals) for which a description beyond DFT-LDA is needed (note however that all other orbital components in the valence will also be modified indirectly by feedback effects of the self-energy associated with the correlated ones). For simplicity, we restrict the discussion here to the case of one 'correlated' atom per unit cell. The orbitals generating the correlated subset need not coincide with basis functions in general[12]. However in the present work, we do choose them as a specific subset $\chi_{a\mathbf{R}}(\mathbf{r})$ of the LMTOs. Hence, $L = \{l, m, \sigma\}$ runs over all orbitals retained in the valence, while $a = \{m, \sigma\}$ runs only over the 'correlated' subset (denoted by $\mathcal{C}$ in the following). The many-body Hamiltonian considered in LDA+DMFT reads:

$$H = H_{KS} - H_{DC} + H_U \tag{5}$$

In this expression, H_{DC} (corresponding to a one-body potential V_{DC}) is a double-counting correction. Indeed, some of the local Coulomb interaction effects are already taken into account in the exchange-correlation energy, and hence in H_{KS}. The many-body terms H_U act in the subset of correlated orbitals only. They correspond to matrix elements of the Coulomb interaction, and will in general involve general 2-particle terms of the form $\sum_{\mathbf{R},abcd} U_{abcd} c_{a\mathbf{R}}^{\dagger} c_{b\mathbf{R}}^{\dagger} c_{d\mathbf{R}} c_{c\mathbf{R}}$. (In the present work however, only density-density terms will be retained: the form of H_U and H_{DC} used in this article is discussed further in Sec. II F).

Let us consider the full Green's function of the solid $G(\mathbf{r}, \mathbf{r}'; \tau - \tau') \equiv -\langle T\psi(\mathbf{r}, \tau)\psi^{\dagger}(\mathbf{r}', \tau')\rangle$, which can be decomposed on the basis set as:

$$G(\mathbf{r}, \mathbf{r}'; \tau - \tau') = \sum_{\mathbf{R}\mathbf{R}'} \sum_{LL'} \chi_{L\mathbf{R}}(\mathbf{r}) \, G_{LL'}(\mathbf{R} - \mathbf{R}', \tau - \tau') \, \chi_{L'\mathbf{R}'}(\mathbf{r}')^{*} \tag{6}$$

DMFT focuses on the local components G_{ab} of the Green's function, on the same atomic site ($\mathbf{R} = \mathbf{R}'$) and within the correlated subspace. The key idea (which can be viewed as a representability assumption) is that G_{ab} can be represented by an effective local model, which is a multi-band generalization of an Anderson impurity model described by the effective action:

$$S = -\int_{0}^{\beta} d\tau \int_{0}^{\beta} d\tau' \sum_{ab} c_a^{\dagger}(\tau) \, [\mathcal{G}_0^{-1}]_{ab}(\tau - \tau') \, c_b(\tau') + \int d\tau \, H_U \tag{7}$$

In this expression, $\mathcal{G}_0$ is the dynamical mean-field, analogous to the familiar Weiss mean-field in classical mean-field theory, the key difference being that here it is a frequency-dependent (i.e energy-scale dependent) quantity. It can also be viewed as the hybridization function which connects the correlated atom (effective impurity) to its environment: $\Delta_{ab}(z) = z\,\delta_{ab} - \epsilon_{ab}^f - [\mathcal{G}_0(z)^{-1}]_{ab}$. In this expression, z is an arbitrary frequency in the complex plane, and ϵ_f is a matrix of effective on-site atomic levels (see sec. II F). The dynamical mean-field $\mathcal{G}_0$ (or Δ) is determined from a self-consistency condition, which expresses that the impurity-model Green's function faithfully represents the local Green's function in the solid projected onto the correlated subset, and hence that the two quantities should coincide. Furthermore, an approximation is made, namely that the many-body self-energy has components on the basis set which are (i) local and (ii) non-zero only in the correlated subspace, so that it also coincides with its impurity model counterpart and takes the form:

$$\Sigma_{LL'}^{\mathbf{R}\mathbf{R}'}(z) = \delta_{\mathbf{R},\mathbf{R}'} \begin{pmatrix} 0 & 0 \\ 0 & \Sigma_{ab}^{imp}(z) \end{pmatrix} \tag{8}$$

The impurity model Green's function and self-energy are defined as:

$$G_{ab}^{imp}(\tau - \tau') \equiv -\langle T c_a^{\dagger}(\tau) c_b(\tau')\rangle_{imp} \quad , \quad \Sigma_{ab}^{imp} \equiv [\mathcal{G}_0^{-1}]_{ab} - [G_{imp}^{-1}]_{ab} \tag{9}$$

in which the average indicated by $\langle ...\rangle_{imp}$ is taken with respect to the effective action (7). The self-consistency condition which determines $\mathcal{G}_0$ can thus be expressed in a concise way as:

$$\hat{P}_{\mathbf{R}}^{\mathcal{C}} \, \hat{G} \, \hat{P}_{\mathbf{R}}^{\mathcal{C}} = \hat{G}_{imp} \tag{10}$$

in which the full Green's function $\hat{G}$ of the solid is projected on a given correlated atom, and onto the correlated subset with the projector:

$$\hat{P}_{\mathbf{R}}^{\mathcal{C}} \equiv \sum_{a} |\chi_{\mathbf{R}a}\rangle\langle\chi_{\mathbf{R}a}| \tag{11}$$

Given (9) and given Dyson's equation relating $\hat{G}$ and Σ, Eq. (10) yields an implicit relation between G_{imp} and $\mathcal{G}_0$. To be fully explicit, let us go through the iterative process (the DMFT loop depicted in Fig. 1) which determine G_{imp}, Σ_{imp} and $\mathcal{G}_0$ self-consistently. Given an initial guess for $\mathcal{G}_0$, the impurity Green's function G_{imp} is calculated using some appropriate 'impurity solver', and the impurity self-energy is obtained as: $\Sigma_{ab}^{imp} \equiv [\mathcal{G}_0^{-1}]_{ab} - [G_{imp}^{-1}]_{ab}$, and used as the only non-zero block of $\Sigma_{LL'}$ (Eq. 8). The Green's function in the solid can then be calculated as:

$$[G^{-1}]_{LL'}(\mathbf{k}, z) = (z + \mu)\delta_{LL'} - H_{LL'}^{KS} + V_{LL'}^{DC} - \Sigma_{LL'}(z) \tag{12}$$

and summed over **k**-points in the Brillouin zone in order to yield the local Green's function on the atomic site associated with the correlated atom as:

$$G_{loc}(z) = \sum_{\mathbf{k}} \left[(z+\mu)\delta_{LL'} - H_{LL'}^{KS} + V_{LL'}^{DC} - \Sigma_{LL'}(z) \right]^{-1} \qquad (13)$$

The block corresponding to the correlated orbitals is extracted from this expression and inverted in order to get an iterated value for the dynamical mean-field, as:

$$[\mathcal{G}_0^{-1}]_{ab} = \Sigma_{imp} + [P^{\mathcal{C}} G_{loc} P^{\mathcal{C}}]^{-1}, \qquad (14)$$

and the DMFT iteration can be pursued. Note that, even though the self-energy matrix has only components in the subspace of correlated orbitals, components of the Green's function corresponding to all valence orbitals $(s, p, \cdots)$ are modified due to the matrix inversion. Hence there is a feedback of correlation effects onto these orbitals as well.

At the end of the DMFT cycle, the resulting Green's function can be considered as a full many-body solution of the Hamiltonian defined by Eq. (5), for a given charge density determining H_{KS}, under the approximation that the corresponding self-energy is taken to be purely local. The charge density can then be recalculated from the Green's function at the end of this cycle, as:

$$\rho(\mathbf{r}) = \sum_{\mathbf{R}\mathbf{R}'} \sum_{LL'} \chi_{L\mathbf{R}}(\mathbf{r}) \, G_{LL'}(\mathbf{R}-\mathbf{R}', \tau-\tau'=0^-) \, \chi_{L'\mathbf{R}'}(\mathbf{r})^* \qquad (15)$$

From this updated charge density, a new Kohn-Sham potential is constructed from (1), and the associated one-particle Schrödinger equation is solved again in order to produce an updated H_{KS}, which serves as a new input for the DMFT cycle. This is indicated as the DFT loop on Fig. 1. Full self-consistency is reached when all local quantities $(G_{imp}, \Sigma_{imp}, \mathcal{G}_0)$ as well as the charge density $\rho(\mathbf{r})$, have converged. Note that the LDA+DMFT self-consistent charge density is affected by correlation effects through the many-body self-energy and that it differs from its LDA self-consistent value $\rho_{LDA}(\mathbf{r})$. Furthermore, it also differs from the charge density associated with the occupied Kohn-Sham orbitals and evaluated with the converged H_{KS} but $\Sigma = 0$ in (15), i.e: $\rho_{KS}(\mathbf{r}) \equiv \sum'_{\mathbf{k}\nu} |\psi_{\mathbf{k}\nu}(\mathbf{r})|^2$. That is, the Kohn-Sham representation is not used for the self-consistent charge density within LDA+DMFT. In the next two sections, we first give a brief reminder of the LMTO formalism and basis-set, and then proceed with the practical evaluation of expression (15) for the charge density in this basis-set.

B. The LMTO basis set

As discussed in detail in section II A, since DMFT emphasizes local correlations, one needs to construct a localized basis set, i.e basis functions which are centered on the atomic positions **R** in the crystal lattice. Up to now, most implementations have used basis sets based on linear muffin-tin orbitals[19] (LMTOs) $\chi_{L\mathbf{R}}(\mathbf{r}) = \chi_L(\mathbf{r}-\mathbf{R})$. These basis sets offer the advantage to carry over the physical intuition of atomic orbitals from the isolated atom to the solid. The LMTO method has been extensively used in electronic structure calculations and thoroughly described in review articles[20,21]. Here we only outline the main features of the LMTO basis set which are relevant to the selfconsistent implementation of the LDA+DMFT scheme.

MT-methods suppose that the crystal potential is spherically symmetric near each atomic site and constant in the interstitial region between atoms. The conventional LMTO method employs a further simplification, the atomic-sphere approximation (ASA), which assumes that the whole space of a crystal is filled with atomic spheres and neglects both the overlap and interstitial spaces. The LMTO basis is constructed from the solution (partial wave) $\phi_{L\mathbf{R}}$ of the spherically symmetric KS potential inside the atomic sphere located at **R** for a certain energy E_ν (typically, the center of gravity of a band) and its energy derivative $\dot{\phi}_{L\mathbf{R}}$. The angular dependence is provided by a spherical harmonic Y_L, corresponding to the orbital and magnetic quantum numbers L). The expression for a linearized MT-orbital is:

$$\chi_{L\mathbf{R}}^{\alpha}(\mathbf{r}) = \phi_{L\mathbf{R}}(\mathbf{r}) + \sum_{L'\mathbf{R}'} \dot{\phi}_{L'\mathbf{R}'}(\mathbf{r}) h_{L'\mathbf{R}'L\mathbf{R}}^{\alpha}, \qquad (16)$$

where the first and second terms in the right-hand side of this equation are usually called the "head" and "tail", respectively. The superscript α designates a particular LMTO representation (the so-called "screened"
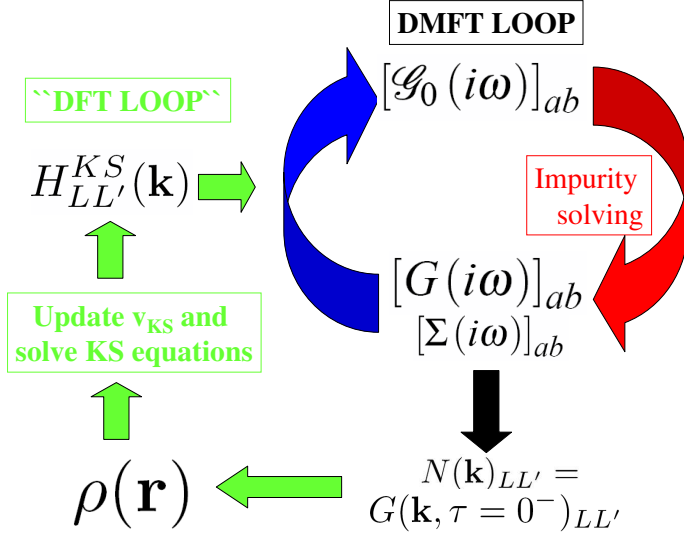
FIG. 1: (Color online). DMFT combined with electronic structure calculations. Starting from a local electronic density $\rho(\mathbf{r})$, the associated Kohn-Sham potential is calculated and the Kohn-Sham equations are solved. The Kohn-Sham hamiltonian $H_{LL'}^{KS}(\mathbf{k})$ is expressed in a localised basis set (e.g LMTOs). A double-counting term is subtracted to obtain the effective one-electron Hamiltonian $H_0 \equiv H^{KS} - H^{DC}$. The local self-energy matrix for the subset of correlated orbitals is obtained through the iteration of the DMFT loop: a multi-orbital impurity model for the correlated subset is solved (red (lighter grey) arrow), containing as an input the dynamical mean-field (or Weiss field $\mathcal{G}_0$). The self-energy Σ_{ab} is combined with H_0 into the self-consistency condition Eqs. (13,14) in order to update the Weiss field (blue (darker grey) arrow). At the end of the DMFT loop, the components of the full, $\mathbf{k}$-dependent, Green's function in the local basis set can be calculated, yielding the momentum-distribution matrix $N(\mathbf{k})_{LL'}$ and the updated charge density $\rho(\mathbf{r})$ as described in Sec. II C. This updated charge density is used to compute the new Kohn-Sham potential until a converged local density is also reached (for the DFT loop). At the same time, the chemical potential must also be adjusted self-consistently with the total number of electrons.

non-orthogonal representation), which is defined by the choice of the envelope functions for the interstitial. We have actually employed here the so-called nearly-orthogonal γ-representation[22], where h^γ is chosen as:

$$h_{L'\mathbf{R}'L\mathbf{R}}^{\gamma} \equiv H_{L'\mathbf{R}'L\mathbf{R}}^{KS} - E_\nu \, \delta_{\mathbf{R}'\mathbf{R}}\delta_{L'L} \tag{17}$$

Using the orthogonality property of the partial wave and its energy derivative $\langle \dot{\phi}_{L\mathbf{R}}|\phi_{L\mathbf{R}}\rangle = 0$ one may easily show[22] that the head of the LMTO in the γ-representation is orthogonal to any LMTO centered on any other site up to a second-order contribution due to the overlap of the energy derivatives of the partial waves. Then the basis can be made completely orthogonal by means of an numerical orthogonalization, for example, the Löwdin transformation[23]. The use of an orthogonal basis is technically simpler when implementing LDA+DMFT (although a non-orthogonal basis may be more advisable in principle since it is expected to reduce the range of interaction terms). A numerical orthogonalization usually introduces undesirable mixing between strongly and weakly correlated states. Because the LMTO basis in the γ representation is already nearly-orthogonal, the inter-orbital mixing are small however.

One of the main advantages of the LMTO technique is the small size of its basis. It can be made even smaller through use of the downfolding procedure[24], which allows to reduce the size of the Hamiltonian by folding down those states which are located well above the valence band. This technique substantially reduces the computational effort, a gain which is especially important in the case of the time-consuming LDA+DMFT calculations. The down-folded LMTO can be expressed as follows:

$$\chi_{L\mathbf{R}}^{\gamma}(\mathbf{r}) = \phi_{L\mathbf{R}}(\mathbf{r}) + \sum_{L'\mathbf{R}'} \dot{\phi}_{L'\mathbf{R}'}(\mathbf{r})h_{L'\mathbf{R}'L\mathbf{R}}^{\gamma} + \sum_{H\mathbf{R}''} \phi_{H\mathbf{R}''}(\mathbf{r})Z_{H\mathbf{R}''L\mathbf{R}}, \tag{18}$$

where L labels "active" orbitals, which are explicitly included in the Hamiltonian, H runs over the set of downfolded orbitals, the matrix Z can be expressed through the structure constants and potential parameters[24]. Following Ref. [24] we neglect the energy dependence of the downfolded orbitals $\phi_{H\mathbf{R}''}(\mathbf{r})$. In

the case of a periodic crystal, one may rewrite expression (18) at each **k**-point in the Brillouin zone as:

$$\chi_L^{\mathbf{k}}(\mathbf{r}) = \phi_L(\mathbf{r}) + \sum_{L'} \dot{\phi}_{L'}(\mathbf{r}) h_{L'L}^{\mathbf{k}} + \sum_H \phi_H(\mathbf{r}) Z_{HL}^{\mathbf{k}}, \tag{19}$$

C. The Calculation of the Charge Density

In this section, we describe the practical implementation of the calculation of the LDA+DMFT charge density in the LMTO basis set. Expression (15) can be rewritten as:

$$\rho(\mathbf{r}) = \sum_{LL'} \sum_{\mathbf{k}} \chi_{L\mathbf{k}}(\mathbf{r}) \, N_{LL'}^{\mathbf{k}} \chi_{L'\mathbf{k}}^*(\mathbf{r}) \tag{20}$$

in which $N_{LL'}^{\mathbf{k}}$ is the **k**-dependent occupancy matrix related to the full Green's function (6) by:

$$N_{LL'}^{\mathbf{k}} \equiv G_{LL'}(\mathbf{k}, \tau = 0^-) = T \sum_n G_{LL'}(\mathbf{k}, i\omega_n) \, e^{i\omega 0^+} \tag{21}$$

The last equality is expressed as a sum over fermionic Matsubara frequencies $\omega_n = (2n+1)\pi/\beta$ corresponding to the temperature $T = 1/\beta$. By inserting the linear MT-orbitals (19) in (20), one can obtain a general formula for the LDA+DMFT charge density in the LMTO framework, which involves simply the calculation of momentum averages of N and of products of N with the hamiltonian matrix h. This expression can be further simplified if the atomic-sphere approximation (ASA) is used, in which the potential is approximated as spherically symmetric within the MT-spheres. In accordance with this approximation, crossed terms between different angular momentum channels can be neglected. Neglecting also the overlap between spheres and using the orthogonality $\langle \phi_L | \phi_{L'} \rangle = \delta_{LL'}$ and $\langle \phi_L | \phi_H \rangle = 0$ between partial waves yields our final expression for the angular-averaged charge density in a given unit cell (valid within the ASA):

$$\rho(r) = \sum_L \left(m_L^{(0)} |\phi_L(r)|^2 + 2m_L^{(1)} \phi_L(r)\dot{\phi}_L(r) + m_L^{(2)} |\dot{\phi}_L(r)|^2 \right) + \sum_H m_H^{(0)} |\phi_H(r)|^2, \tag{22}$$

In this expression, the moments $m^{(i)}$'s are defined from the **k**-dependent occupancy matrix and LMTO first-order Hamiltonian h (for a given atom **R**) as:

$$\begin{aligned}
m_L^{(0)} &\equiv \sum_{\mathbf{k}} N_{LL}^{\mathbf{k}} = \langle \mathrm{tr} N \rangle_{\mathbf{k}} \\
m_H^{(0)} &\equiv \sum_{\mathbf{k}} \sum_{LL'} Z_{HL}^{\mathbf{k}} N_{LL'}^{\mathbf{k}} Z_{L'H}^{\mathbf{k}} = \langle \mathrm{tr}(Z_H N Z_H) \rangle_{\mathbf{k}} \\
m_L^{(1)} &\equiv \sum_{\mathbf{k}} \sum_{L'} N_{LL'}^{\mathbf{k}} h_{L'L}^{\mathbf{k}} = \langle \mathrm{tr}(Nh) \rangle_{\mathbf{k}} \\
m_L^{(2)} &\equiv \sum_{\mathbf{k}} \sum_{L'L''} h_{LL'}^{\mathbf{k}} N_{L'L''}^{\mathbf{k}} h_{L''L}^{\mathbf{k}} = \langle \mathrm{tr}(hNh) \rangle_{\mathbf{k}}
\end{aligned} \tag{23}$$

Expressions (22,23) are similar to those used in the context of usual DFT in the LMTO-ASA formalism, the key difference being that in the DMFT context, the momentum-distribution matrix $N^{\mathbf{k}}$ is computed from the many-body Green's function according to (20) instead than from filling independent orbitals as in the KS representation of the density. In practice, the moments (23) are computed at the end of the DMFT cycle and then passed on into the LMTO electronic structure part of the program, where a new total charge density is computed according to formula (22), as indicated on Fig. 1.

D. The Total Energy Functional

In order to discuss total energy calculations in the LDA+DMFT framework, it is best to use a formulation of this scheme in terms of a (free-) energy functional. Kotliar and Savrasov[10,25,26] have introduced for this purpose a ("spectral-density-") functional of both the total charge density $\rho(\mathbf{r})$ and the on-site Green's function in the correlated subset: $G_{ab}^{\mathbf{RR}}$ (denoted G_{ab} for simplicity in the following). Let us

emphasize that these quantities are independent, since G_{ab} is restricted to local components and to a subset of orbitals so that $\rho(\mathbf{r})$ cannot be reconstructed from it. The functional is constructed by introducing source terms $l(\mathbf{r}) = v_{KS}(\mathbf{r}) - v_c(\mathbf{r})$ and $\Delta\Sigma_{ab}(i\omega_n)$ coupling to the operators $\psi^\dagger(\mathbf{r})\psi(\mathbf{r})$ and to $\sum_{\mathbf{R}} \chi_a^*(\mathbf{r}-\mathbf{R})\psi(\mathbf{r},\tau)\psi^\dagger(\mathbf{r}',\tau')\chi_b(\mathbf{r}'-\mathbf{R}) = c_{a\mathbf{R}}(\tau)c_{b\mathbf{R}}^\dagger(\tau')$, respectively. Furthermore, the Luttinger-Ward[27] part of the functional is approximated by that of the on-site local many-body Hamiltonian $H_U - H_{DC}$ introduced above. This yields:

$$\Omega[\rho(\mathbf{r}), G_{ab}; v_{KS}(\mathbf{r}), \Delta\Sigma_{ab}]_{LDA+DMFT} =$$
$$-\mathrm{tr}\,\ln[i\omega_n + \mu + \tfrac{1}{2}\nabla^2 - v_{KS}(\mathbf{r}) - \chi^*.\Delta\Sigma.\chi] - \int d\mathbf{r}\,(v_{KS} - v_c)\rho(\mathbf{r}) - \mathrm{tr}\,[G.\Delta\Sigma] +$$
$$+\tfrac{1}{2}\int d\mathbf{r}\,d\mathbf{r}'\rho(\mathbf{r})\,\frac{e^2}{|\mathbf{r}-\mathbf{r}'|}\,\rho(\mathbf{r}') + E_{xc}[\rho(\mathbf{r})] + \sum_{\mathbf{R}}\left(\Phi_{imp}[G_{ab}^{\mathbf{RR}}] - \Phi_{DC}[G_{ab}^{\mathbf{RR}}]\right)$$

In this expression, $\chi^*.\Delta\Sigma.\chi$ denotes the "upfolding" of the local quantity $\Delta\Sigma$ to the whole solid: $\chi^*.\Delta\Sigma.\chi = \sum_{\mathbf{R}}\sum_{ab}\chi_a^*(\mathbf{r}-\mathbf{R})\Sigma_{ab}(i\omega_n)\chi_b(\mathbf{r}'-\mathbf{R})$. Variations of this functional with respect to the sources $\delta\Omega/\delta v_{KS} = 0$ and $\delta\Omega/\delta\Sigma_{ab} = 0$ yield the standard expression of the local density and local Green's function in terms of the full Green's function of the solid, which we have used in the previous section:

$$\rho(\mathbf{r}) = \langle \mathbf{r}|\hat{G}|\mathbf{r}\rangle \;,\;\; G_{ab}(i\omega_n) = \langle \chi_{a\mathbf{R}}|\hat{G}|\chi_{b\mathbf{R}}\rangle \tag{24}$$

with:

$$\hat{G} = \left[i\omega_n + \mu + \frac{1}{2}\nabla^2 - v_{KS}(\mathbf{r}) - \chi^*.\Delta\Sigma.\chi\right]^{-1} \tag{25}$$

Note that these expressions, as well as the functional, are written here in a manner which does not refer explicitly to a specific basis set. The formalism does depend, however, on the choice of localized orbitals defining the correlated subspace.

From these relations, the Legendre multiplier functions v_{KS} and $\Delta\Sigma$ can be eliminated in terms of ρ and G_{ab}, so that a functional of these local observables only is obtained:

$$\Gamma_{LDA+DMFT}[\rho, G_{ab}] = \Omega_{LDA+DMFT}\left[\rho(\mathbf{r}), G_{ab}; l[\rho, G], \Delta\Sigma[\rho, G]\right] \tag{26}$$

Extremalisation of this functional with respect to ρ ($\delta\Gamma/\delta\rho = 0$) and G_{ab} ($\delta\Gamma/\delta G_{ab} = 0$) yields the expression of the Kohn-Sham potential and self-energy correction at self-consistency:

$$v_{KS}(\mathbf{r}) = v_c(\mathbf{r}) + \int d\mathbf{r}'\frac{e^2}{|\mathbf{r}-\mathbf{r}'|}\rho(\mathbf{r}') + \frac{\delta E_{xc}}{\delta\rho(\mathbf{r})} \tag{27}$$

$$\Delta\Sigma_{ab} = \frac{\delta\Phi_{imp}}{\delta G_{ab}} - \frac{\delta\Phi_{DC}}{\delta G_{ab}} \equiv \Sigma_{ab}^{imp} - V_{ab}^{DC} \tag{28}$$

Hence, one recovers from this functional the defining equations of the LDA+DMFT combined scheme detailed in the previous section, including self-consistency over the local density (24).

The free-energy (24,26) leads to the following expression of the total energy:

$$E_{LDA+DMFT} = \sum_{\mathbf{k},LL'} H_{LL'}^{KS}(\mathbf{k})N_{LL'}^{\mathbf{k}} + \int d\mathbf{r}[v_c(\mathbf{r}) - v_{KS}(\mathbf{r})]\rho(\mathbf{r}) + \tag{29}$$
$$+\tfrac{1}{2}\int d\mathbf{r}d\mathbf{r}'\rho(\mathbf{r})\frac{e^2}{|\mathbf{r}-\mathbf{r}'|}\rho(\mathbf{r}') + E_{xc}[\rho] + \langle H_U \rangle - E_{DC}.$$

The sum of the first four terms in this expression is reminiscent of the expression of the total energy in DFT, $E_{DFT}[\rho(\mathbf{r})]$, evaluated at the self-consistent charge density $\rho(\mathbf{r})$, except for the fact that the many-body (LDA+DMFT) momentum-distribution matrix enters the first term. Instead, within DFT, the first term reads $\sum_{\mathbf{k}\nu}' \varepsilon_{\mathbf{k}\nu}^{KS}$, where the prime indicates that the sum is to be taken only over occupied KS orbitals (filled up to μ_{KS}, adjusted so that the total number of electrons is obtained. Hence, in practice, the total energy can be calculated as:

$$E_{LDA+DMFT} = \left(E_{DFT}[\rho(\mathbf{r})] - \sum_{\mathbf{k}\nu}' \varepsilon_{\mathbf{k}\nu}^{KS}\right) + \sum_{\mathbf{k},LL'} H_{LL'}^{KS}(\mathbf{k})N_{LL'}^{\mathbf{k}} + \langle H_U \rangle - E_{DC} =$$
$$= E_c[\rho] + E_H[\rho] + E_{xc}[\rho] + \sum_{\mathbf{k},LL'} H_{LL'}^{KS}(\mathbf{k})N_{LL'}^{\mathbf{k}} + \langle H_U \rangle - E_{DC} \tag{30}$$

The first three terms are the crystal, Hartree and exchange-correlation energy, respectively. The last three terms coincide with the energy associated with the many-body Hamiltonian $H_{KS}-H_{DC}+H_U$. the interaction energy $\langle H_U \rangle$ may be computed either directly from the expression of the Hamiltonian H_U (for example, by evaluating the correlations $\langle n_a n_b \rangle$ within the impurity solver, which is easy e.g when using quantum Monte Carlo). Alternatively, the Migdal formula $\langle H_U \rangle = \mathrm{Tr}\,(\Sigma G)/2$ can be applied, as actually done in this work when using the Hubbard-I approximation and described in the next section.

E.   Some practical aspects of total energy calculations

An accurate evaluation of the **k**-dependent occupancy matrix (21) is necessary in order to obtain the correct charge density (22) and total energy (29). If calculations are performed at finite temperature then this requires a careful summation of the high-frequency tails of the Green's function in (21). In addition, the formula (29) for the total energy contains the Migdal contribution, which is also computed through the corresponding summation over the Matsubara frequencies:

$$\langle H_U \rangle = \frac{1}{2}\mathrm{Tr}\left[\hat{G}(\tau=0^-)\hat{\Sigma}(\tau=0^-)\right] = \frac{T}{2}\mathrm{Tr}\sum_n G(i\omega_n)\Sigma(i\omega_n)e^{i\omega_n 0^+} \tag{31}$$

Here both the Green's function and self-energy contain high-frequency tails, which should be properly taken into account in the evaluation of the sum over ω_n. In Refs. [28,29,30] evaluation of the Matsubara sums over the high-frequency tails have been treated in details, however the approach proposed there is applicable only if the self-energy is calculated by means of an analytic technique. Due to the wide spread of numerical DMFT solvers (for example, quantum Monte Carlo), it is highly desirable to have a "solver-independent" technique for accurate evaluations of Matsubara sums, which we describe in this chapter.

We shall isolate the first two terms in the high-frequency expansion of the self-energy matrix, which is thus decomposed as:

$$\hat{\Sigma}(i\omega_n) = \hat{\Sigma}(i\infty) + \frac{\hat{A}}{i\omega_n} + \hat{\Sigma}_{num}(i\omega_n) \equiv \hat{\Sigma}_{an}(i\omega_n) + \hat{\Sigma}_{num}(i\omega_n) \tag{32}$$

In this expression, the numerically determined $\hat{\Sigma}_{num}(i\omega_n) = \hat{\Sigma}(i\omega_n) - \hat{\Sigma}_{an}(i\omega_n)$ will be neglected for Matsubara frequencies larger than a certain cutoff ω_{cut}, while the high-frequency contribution $\hat{\Sigma}_{an}(i\omega_n) \equiv \hat{\Sigma}(i\infty) + \hat{A}/i\omega_n$ will be treated analytically when performing frequency sums. One may extract the matrices $\hat{\Sigma}(i\infty)$ and $\hat{A}$ (the latter being actually diagonal in the present case) from the real and imaginary parts of the self-energy at the cutoff frequency $\hat{\Sigma}(i\omega_{cut})$, or use a more sophisticated way for fitting them. A similar decomposition can be applied to the Green's function:

$$\hat{G}(\mathbf{k}, i\omega_n) = \quad \hat{G}_{num}(\mathbf{k}, i\omega_n) + \hat{G}_{an}(\mathbf{k}, i\omega_n) \tag{33}$$
$$= \quad \hat{G}_{num}(\mathbf{k}, i\omega_n) + \left[(i\omega_n + \mu)\hat{I} - \hat{H}^{KS} + \hat{V}^{DC} - \hat{\Sigma}(i\infty)\right]^{-1},$$

where $\hat{G}_{num}(\mathbf{k}, i\omega_n) = \hat{G}(\mathbf{k}, i\omega_n) - \hat{G}_{an}(\mathbf{k}, i\omega_n)$ is again zero for Matsubara frequencies larger than the cutoff frequency. In the analytical part of the Green's function it is sufficient to keep only the dominant term in the self-energy $\hat{\Sigma}(i\infty)$. Then the matrix $\mu + \hat{V}^{DC} - \hat{H}^{KS} - \hat{\Sigma}(i\infty)$ is Hermitian, and we designate its eigenvectors and eigenvalues as $|X_m^{\mathbf{k}}\rangle$ and $\lambda_m^{\mathbf{k}}$, respectively, so that:

$$\hat{G}(\mathbf{k}, i\omega_n) = \hat{G}_{num}(\mathbf{k}, i\omega_n) + \sum_m \frac{|X_m^{\mathbf{k}}\rangle\langle X_m^{\mathbf{k}}|}{i\omega_n + \lambda_m^{\mathbf{k}}}. \tag{34}$$

In order to evaluate the frequency sum in (21) we carry out the summation of $\hat{G}_{num}$ up to the cutoff frequency, while other frequency sums are performed analytically. By inserting (32) and (34) in the formula

for the Migdal energy (31) one obtains the following expressions of practical use:

$$\langle H_U \rangle = \langle H_U \rangle^{(1)} + \langle H_U \rangle^{(2)} + \langle H_U \rangle^{(3)}, \tag{35}$$

$$\langle H_U \rangle^{(1)} = \frac{T}{2} \sum_{\mathbf{k}} \sum_{|\omega_n| < \omega_{cut}} \left[\hat{G}_{an}(\mathbf{k}, i\omega_n) \hat{\Sigma}_{num}(i\omega_n) + \hat{G}_{num}(\mathbf{k}, i\omega_n) \hat{\Sigma}(i\omega_n) \right],$$

$$\langle H_U \rangle^{(2)} = \frac{1}{2} \sum_{\mathbf{k}} \sum_{m} \frac{\langle X_m^{\mathbf{k}} | \hat{\Sigma}(i\infty) | X_m^{\mathbf{k}} \rangle}{1 + e^{-\beta \lambda_m^{\mathbf{k}}}},$$

$$\langle H_U \rangle^{(3)} = \frac{1}{4} \sum_{\mathbf{k}} \sum_{m} \frac{\langle X_m^{\mathbf{k}} | \hat{A} | X_m^{\mathbf{k}} \rangle}{\lambda_m^{\mathbf{k}}} \frac{1 - e^{\beta \lambda_m^{\mathbf{k}}}}{1 + e^{\beta \lambda_m^{\mathbf{k}}}},$$

The Hubbard-I quantum impurity solver[15] employed in the present work is not constrained to the Matsubara frequencies, and it can in fact be equally well used for calculating the self-energy at any general complex energy. Hence at zero temperature one may easily rewrite frequency sums in the expressions for the occupancy matrix (21) and Migdal energy (29) in a form, which is suitable for a summation over the poles of the GF (and the self-energy in the case of Migdal energy) on the real axis:

$$N_{LL'}^{\mathbf{k}} = \frac{1}{2\pi i} \oint G_{LL'}(\mathbf{k}, z), \tag{36}$$

$$\langle H_U \rangle = \frac{1}{4\pi i} \oint Tr\left[G(z)\Sigma(z)\right] dz, \tag{37}$$

where integration is performed over the contour in the complex energy plane, which encloses valence-band energy poles. Therefore, within the Hubbard-I approach and at zero temperature one may completely avoid the problem of summation of the high-frequency tails. We have applied both the finite temperature Matsubara temperature summation and contour integration techniques in the fully self-consistent LDA+DMFT calculations of γ-Ce and Ce_2O_3.

F. Choice of interaction vertex, impurity solver, and double-counting

The last term in Eq.(5), H_U gives the many-body interaction terms acting in the subset of correlated orbitals. They correspond to matrix elements of the Coulomb interaction, and will in general involve arbitrary 2-particle terms $U_{abcd} c_a^\dagger c_b^\dagger c_d c_c$. There the 4-index matrix U_{abcd} is defined for a f-shell by four Slatter integrals F^0, F^2, F^4, and F^6. In the quasiatomic (spherical) approximation the Slatter integrals can be expressed through only two parameters U and J (see Ref. 31). In addition to the spherical approximation one often makes a further simplification and keeps only density-density interactions (we employ this simplification in the current version of our Hubbard-I impurity solver, though in general it is not necessary). We shall limit ourselves here to this case and use:

$$H_U = \frac{1}{2} \sum_{\mathbf{R}} \sum_{mm'\sigma\sigma'} U_{mm'}^{\sigma\sigma'} \hat{n}_{\mathbf{R}m}^{\sigma} \hat{n}_{\mathbf{R}m}^{\sigma'} \tag{38}$$

with the effective two-index matrix derived from a more general 4-index form as follows:

$$U_{mm'}^{\uparrow\downarrow} = U_{mm'mm'} \ , \ U_{mm'}^{\uparrow\uparrow} = U_{mm'}^{\downarrow\downarrow} = U_{mm'mm'} - U_{mm'm'm} \tag{39}$$

Next, we discuss the impurity solver that we use in practice in this article. Both materials that we shall consider for illustrative purposes (Ce_2O_3 and γ-Ce) have nominally an f^1 configuration, and the f-electron is actually localized. The practical solution of the DMFT equation can be simplified considerably by choosing an approximate 'impurity solver' appropriate to this localized character. The simplest of those is the 'Hubbard-I' approximation. In this approximation, the self-energy is approximated by its 'atomic limit', in which the hybridization function $\Delta_{ab}(z)$ is neglected. One should still correctly identify however the effective atomic levels entering the Weiss dynamical mean-field $[\mathcal{G}_0^{-1}]_{mm'} = z - \epsilon_{mm'} - \Delta_{mm'}(z)$ (with

$m, m' \in \mathcal{C}$). For this purpose, we can perform a high-frequency expansion of the self-consistency equation (13,14) and request that $\Delta(z)$ vanishes at high frequency, which leads to:

$$\epsilon_{mm'} = -\mu \, \delta_{mm'} + \sum_{\mathbf{k}} H_{mm'}^{KS}(\mathbf{k}) - V_{mm'}^{dc} \tag{40}$$

In the present case, this is actually a diagonal matrix of effective atomic levels $\epsilon_{mm'} = \epsilon_m \delta_{mm'}$. These levels must be recalculated iteratively, as they change upon updating the chemical potential. Hence, the effective atomic Hamiltonian reads:

$$H_{at}^{eff} = \sum_{\sigma, m \in \mathcal{C}} \epsilon_m \, \hat{n}_{m\sigma} + H_U \tag{41}$$

This Hamiltonian can be diagonalized, yielding (many-body) energy levels E_A's and eigenstates $|A\rangle$, from which the atomic Green's function can be constructed as:

$$[G_{at}(z)]_{mm'} = \delta_{mm'} \frac{1}{\mathcal{Z}} \sum_{AB} \frac{|\langle A|d_m^\dagger|B\rangle|^2}{z + E_B - E_A}(e^{-\beta E_A} + e^{-\beta E_B}) \ , \ \ \mathcal{Z} = \sum_A e^{-\beta E_A} \tag{42}$$

The atomic self-energy is obtained from $\Sigma_{at} = (z - \epsilon_m)\delta_{mm'} - G_{at}^{-1}$. This leads to the following expression for the Green's function of the full solid, in the Hubbard-I approximation:

$$[G(\mathbf{k}, z)^{-1}]_{LL'} = (\mu + \epsilon_L + V^{dc})\delta_{LL'} - H_{LL'}^{KS}(\mathbf{k}) + [G_{at}^{-1}(z)]_{LL'} \tag{43}$$

$$= [G_{at}^{-1}(z)]_{LL'} - \widetilde{H}_{LL'}^{KS}(\mathbf{k}) \tag{44}$$

in which $\widetilde{H}_{LL'}^{KS} = H_{LL'}^{KS}(\mathbf{k}) - \langle H_{LL'}^{KS}(\mathbf{k})\rangle_{\mathbf{k}}$ for $L, L' \in \mathcal{C}$ and $\widetilde{H}_{LL'}^{KS} = H_{LL'}^{KS}(\mathbf{k})$ otherwise (i.e. $\widetilde{H}^{KS}$ is the non-local, inter-atomic part of the KS Hamiltonian). Within the Hubbard-I approximation, the LDA+DMFT loop takes the following form. Starting from H^{KS} at a given stage of the iteration, the effective atomic levels are calculated according to (40) and the local atomic Green's function calculated by diagonalizing the effective atomic Hamiltonian (41). The full Green's function is then formed as (44) and the momentum distribution matrix $N_{LL'}^{\mathbf{k}}$ calculated. The chemical potential is then updated so that $\sum_{\mathbf{k},L} N_{LL}^{\mathbf{k}}$ yields the appropriate total number of electrons, and the updated charge density is obtained by calculating the moments as described in Sec. II C. The KS equations are then solved to yield a new H^{KS} and this process is iterated until convergence of both $\rho(\mathbf{r})$ and of the effective atomic levels ϵ_m.

Finally, we discuss the "double-counting" correction H_{DC}. This correction must be introduced, since the contribution of interactions between the correlated orbitals to the total energy is already partially included in the exchange-correlation potential derived from E_{xc}. Unfortunately, it is not possible to derive this term explicitly, since the energy within DFT is a functional of the total electron density, which combines all orbitals in a non-linear manner. In practice, the most commonly used form of the double-counting term is (for other choices, see e.g [32]):

$$H_{DC} = \sum_{\mathbf{R}\sigma ab} V_{ab\sigma}^{DC} c_{a\sigma}^\dagger c_{b\sigma}$$

$$V_{ab\sigma}^{DC} = \delta_{ab}\left[U(N_f - \frac{1}{2}) - J(N_f^\sigma - \frac{1}{2})\right], \tag{45}$$

where $N_f = N_f^\uparrow + N_f^\downarrow$ is the total occupancy in the correlated shell $\mathcal{C}$ (i.e the f-shell in practice in this article). One issue arises here, which is which value of N_f must actually be used in (45). When solving the DMFT equations with a numerically exact solver, it would seem (from the previous functional-based derivation) that N_f should be the occupancy of the f-shell obtained at self-consistency. However, we have found this to be inappropriate when using the Hubbard-I approximation as a solver and leading to too small equilibrium volumes. Instead, we note that the Hubbard-I solver treats an effective isolated atom, which has this a frozen occupancy taking integer values at $T = 0$. Hence, a natural choice within Hubbard-I is to choose this frozen integer occupancy in the double-counting correction. For the f^1 materials in the paramagnetic phase treated in this article ($N_f^\uparrow = N_f^\downarrow = 1/2$), so that the Hund's coupling therefore drops out of H_{DC} which reads simply:

$$V_{ab\sigma}^{DC} = \delta_{ab}\frac{U}{2},$$

This also implies that the U-dependent contribution of the double counting correction in the total energy actually vanishes for f^1 compounds within the Hubbard-I approximation, and for this choice of double-counting potential.

III.   FULLY SELF-CONSISTENT LDA+DMFT CALCULATIONS OF CE_2O_3 AND γ-CERIUM

We have applied the LMTO-based fully self-consistent LDA+DMFT technique in order to calculate the density of states and thermodynamical properties of the cerium sesquioxide Ce_2O_3 and pure Ce in its γ-phase. The main aim of these calculations is to validate our implementation of the fully self-consistent LDA+DMFT technique, as well as to study the impact of the charge self-consistency on spectral and thermodynamic properties. Hence, it is desirable to avoid additional complications due to the use of sophisticated and computationally expensive quantum impurity solvers. While the Ce $4f$ band cannot be properly modeled by conventional LDA techniques, due to its essentially atomic-like (localized) character, the electronic correlations on the $4f$ shell can be treated by means of the simplest "strong-coupling" Hubbard-I (HI)[15] approximate impurity solver, described in the previous section. Therefore for our purposes these two strongly correlated rare-earth compounds, with nominally one localized f-electron, appear to be a suitable choice. Both pure cerium and the oxide Ce_2O_3 are well studied theoretically and experimentally, because they raise questions of fundamental interest (e.g. concerning the α-γ transition in Ce[33,34]) as well as for technological reasons (for example, Ce-oxides are used for oxygen storage in solid-oxide fuel cells[16]).

A. Ce_2O_3

The electronic properties of Ce_2O_3 are largely determined by the localized Ce $4f$ orbitals. This compound is an insulator with a gap of about 2.5 eV. At low temperatures, Ce_2O_3 orders antiferromagnetically, with a Néel temperature (9 K) which is several orders of magnitude smaller than the gap. It is thus clear that the antiferromagnetic order is not the driving force behind the insulating character of this material. Rather, strong correlations open up a gap among the $4f$ states, and this compound can therefore be viewed as an f-electron based Mott insulator. As for all such materials, it is a challenge for conventional electronic structure calculations to describe the opening of the correlation-induced gap. The Kohn-Sham spectrum of DFT-LDA is metallic, with $4f$ states at the Fermi level. An insulating state of Ce_2O_3 has been obtained within the self-interaction correction approach[35], albeit with a strongly overestimated value for the band gap. In the antiferromagnetic phase, the LDA+U method can be employed[36,37,38,39], as well as the hybrid functional approach[40]. In this article, we focus on the paramagnetic phase, at low temperature just above the Néel ordering temperature. Dynamical mean-field theory and the Hubbard-I approximation used here allows us to describe the opening of the Mott gap and the existence of local moments in the paramagnetic phase, due to the quasi-localized $4f$ electrons.

1.   Details of the calculational setup

We have calculated the density of states and spectral density of Ce_2O_3 oxide in the hexagonal lattice structure (space group $P\bar{3}m1$) at experimental volume (a =3.890 Å, c/a=1.557[41]). Empty spheres have been introduced in order to make the structure more close packed. In the computation of the spectra we have included the $6s$, $5d$ and $4f$ orbitals of Ce, the $2p$ orbitals of oxygen and the $1s$ orbitals on the empty spheres in the basis set as active LMTOs. In addition, the $6p$ orbital of Ce, the $3s$ and $3d$ oxygen orbitals, and the $2p$ orbitals on the empty spheres have been downfolded. In the total energy calculations it is necessary to include the Ce semicore $5p$ orbital[16] as well. The LMTO code employed by us is not able to treat semicore states in a separate panel, hence in the total energy calculations we have excluded the Ce $6p$ orbitals from the basis. It is important to include the $6p$ orbitals in order to obtain accurate spectra; however, as will be shown in the next chapter on γ-Ce, for total energy calculations they are less significant.

In the self-consistent LDA+DMFT calculations we have employed 62 $\mathbf{k}$−points in order to carry out the integration over the irreducible Brillouin zone of the hexagonal lattice, the energy integration has been carried out on a semicircular contour of depth 2 Ry comprising 40 energy points. In order to obtain the local and $\mathbf{k}$-resolved spectral functions, the self-energy and Green's function were directly computed on the real axis, with 394 $\mathbf{k}$−points used for the integration over the irreducible Brillouin zone.

In order to estimate the value of the screened on-site Coulomb interaction we have performed constrained LSDA calculations[42] both, by fixing the f−electron occupancy and by adding a constrained potential acting on the f-electrons on one Ce atom. Depending on whether the constrained charge or potential approach was used we obtained quite different values of the parameter U, varying from 5.5 to 8 eV. The previous theoretical estimates of Refs. [34,43] of the U value in pure Ce metal put it in the range between 5 and 6 eV, while in the LDA+U calculations of Refs. [38,39] the best agreement between the calculated equilibrium
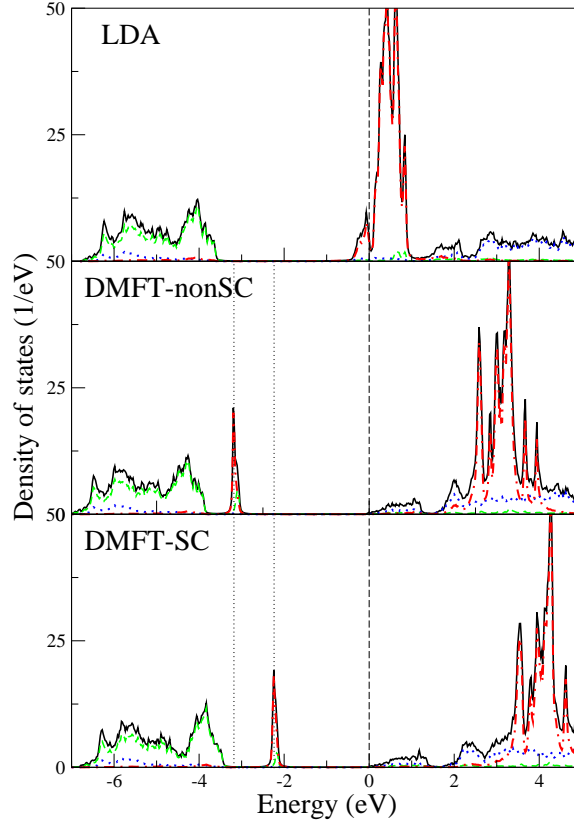
FIG. 2: (Color online). The LMTO Ce_2O_3 DOS calculated within DFT-LDA, the LDA+DMFT with the fixed LDA charge density (DMFT-nonSC), and the LDA+DMFT fully self-consistent over the charge density (DMFT-SC) schemes. The black (solid), green (dashed), blue (dotted) and red (dash-dotted) curves are the total, O, Ce$-d$ and Ce$-f$ DOS, respectively. The vertical dashed line indicates the position of the chemical potential, while the vertical dotted lines indicate positions of the lower Hubbard bands in DMFT-nonSC and DMFT-SC, respectively.

volume and experiment was achieved for a value of the effective $U_{\mathrm{eff}} = U - J$ of about 6 eV. Thus, in our calculations we have fixed the value of $U - J$ to 6 eV, while the value of J=0.46 eV, which depends less crucially than U on the proper treatment of screening in a material, has been taken from the constrained LDA calculations.

We have employed three calculational schemes, for comparison purposes: the conventional LDA, the (non self-consistent) LDA+DMFT with fixed LDA charge density (DMFT-nonSC), and the LDA+DMFT technique with full self-consistency over the charge density (DMFT-SC). In the case of DMFT-nonSC, we carried out DMFT iterations until convergence in the self-energy and chemical potential is reached. In the case of DMFT-SC, additional convergence criteria with respect to the total energy and charge density were employed as well.

2. *Spectral functions and correlated 'bandstructure'*

The orbitally-resolved local density of states (DOS) - or spectral functions-, defined as:

$$A_L(\omega) \equiv -\frac{1}{\pi} \operatorname{Im} \sum_{\mathbf{k}} \mathrm{G_{LL}}(\mathbf{k}, \omega + \mathrm{i}0^+) \tag{46}$$

	μ	C_{KS}^f	$\langle H^f \rangle$	V_{DC}	$\langle \epsilon_f \rangle$
DMFT-nonSC	1.19	1.52	1.18	-3.00	-3.01
DMFT-SC	1.15	2.76	2.18	-3.00	-1.97

TABLE I: The chemical potential, parameter C of the KS f band, double counting and f level positions in the DMFT-nonSC and DMFT-SC approaches (in eV).

are displayed in Fig. 2 for all three methods (LDA, DMFT-nonSC, and DMFT-SC). First, one may notice that conventional LDA calculations place the Ce $4f$-band in the vicinity of the Fermi level, therefore predicting Ce_2O_3 to be a metal. Both the DMFT-nonSC and DMFT-SC approaches correctly predict Ce_2O_3 to be a Mott insulator, where the f-band is split due to the local Coulomb interaction into occupied lower Hubbard bands, and empty upper Hubbard bands. One may notice a significant shift of the positions of the Hubbard bands in the DMFT-SC DOS with respect to the DMFT-nonSC picture. The value of the band gap in Ce_2O_3 is equal to 3.10 eV and 2.13 eV within the DMFT-nonSC and DMFT-SC approaches, respectively. The latter value is in good agreement with the experimental measurements of the optical gap in Ce_2O_3 (2.4 eV, Ref. [44]), while the fixed charge (non-SC) calculations lead to a strong overestimation of the gap. The total occupancy of the f-shell is rather weakly affected by the local Coulomb interaction. The occupancy of the f shell in Ce_2O_3 is equal to 1.145, 1.174, and 1.167 according to the LDA, DMFT-nonSC and DMFT-SC calculations, respectively.

In order to better understand the observed difference between the position of the lower Hubbard band in the non-SC and SC methods, we use the expression (40) of the effective atomic levels within the Hubbard-I approximation, established in the previous section. This yields directly the position of the lower Hubbard band (and of the upper Hubbard band, which is shifted upwards by an energy U) since, for both materials, the f shell of the isolated atom contains just one electron. The effective level position for the m-th orbital component of the $4f$ shell reads:

$$\epsilon_m = -\mu + \sum_{\mathbf{k}} \hat{H}_{mm}^{KS}(\mathbf{k}) - V_{DC}, \tag{47}$$

The double counting term used in the present work reads: $V_{DC} = U(N_f - 1/2) - J(N_f - 1)/2$ and since we set $N_f = 1$ in this expression (as explained in the previous section), we see that the double counting correction term is the same for both the DMFT-nonSC and DMFT-SC approaches. Thus, the difference in the value of the band gap cannot be blamed on the double counting. Therefore, in the Hubbard-I approximation, and for a given local Coulomb interaction, the factor which determines the positions of the lower Hubbard band is the momentum average of H_{KS}, i.e essentially the centre of gravity of the KS f-band (the second term in the right-hand side of expression (47)).

In Table I we list the chemical potentials, the LMTO parameter C^f of the Ce f band (which can be interpreted as the center of a "pure" (unhybridized) KS band), the Hamiltonian integrated over the BZ, the value of the double counting correction and the level position. The brackets $\langle ... \rangle$ in Table I designate an average over the magnetic quantum number m within the f-shell. It is important to realize, that while in the case of DMFT-nonSC, the parameters C_{KS}^f and H^f are just obtained within the conventional LDA, in DMFT-SC it is obtained from the solution of the KS equations with a potential calculated from the self-consistent LDA+DMFT charge density, which differs from the LDA one. One may notice that the KS band structure computed from the DMFT charge density is substantially different from the LDA one, as the centerweight of the f band is shifted by 1.24 eV upwards. This change in the KS band structure is reflected in the values of the Hamiltonian $\langle H^f \rangle$, and, finally, in the positions of the DMFT Hubbard bands, which are determined by the level position ϵ_m. Hence one observes a clear impact of the charge-density self-consistency on the LDA+DMFT electronic structure: changes in the charge density due to DMFT lead to a modification of the KS band structure, which in turn affects the final LDA+DMFT electronic structure. The result is a reduction of the band gap by almost 1 eV. A direct connection between the KS and DMFT electronic structures is especially evident in the present case due to the simplicity of the HI technique, where the position of the LHB is linked to the KS Hamiltonian through the simple relation (47).

Since the Hubbard-I approximation employed here does not describe lifetime effects of the correlated states, the momentum-resolved Green's function still has well-defined poles (in other words, excitations corresponding to the lower and upper Hubbard bands have infinite lifetime). The dispersion of the corresponding upper and lower Hubbard bands of Ce_2O_3 as a function of momentum is displayed in Fig. 3, as obtained with fully self-consistent LDA+DMFT. The LHB shows virtually no dispersion and forms a narrow, atomic-like level
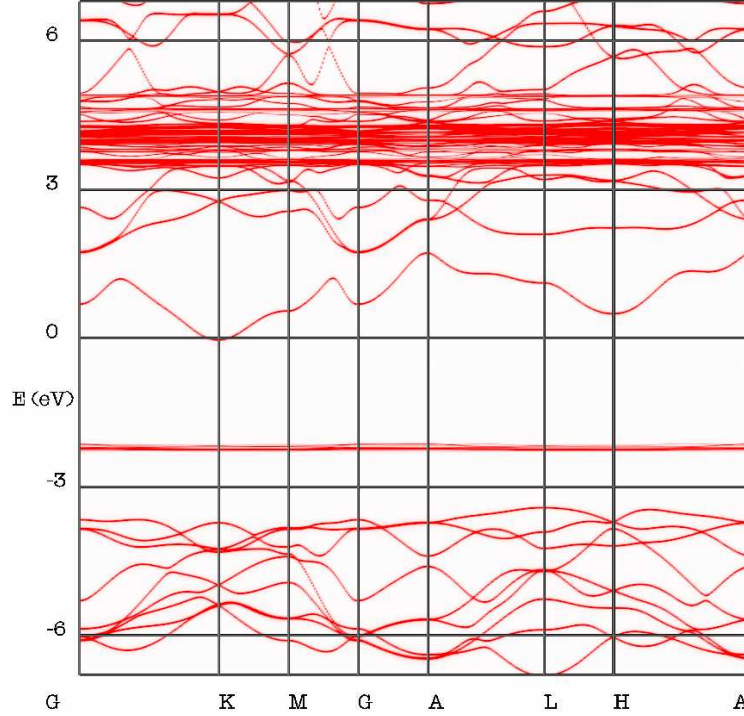
FIG. 3: (Color online). The LMTO fully self-consistent LDA+DMFT **k**-resolved spectral function of Ce_2O_3.

in the gap between the oxygen p and Ce d band. The UHB is essentially a set of atomic-like "multiplet" states, while one may still notice some evidence of weak hybridization between the d band and the UHB[62] .

3. Total energy calculations

The total energy calculations have been carried out by keeping the experimental c/a ratio and using the same setup as in the calculations of the spectra, apart from modifications in the basis, where the $5p$ Ce semicore states were included instead of the $6p$ orbitals. Without the $5p$ semicore states there is no minimum of the total energy vs. volume curve in the range of lattice parameters between 3.60 and 4.2 Å. As in the calculations of spectra, we have employed both the fully self-consistent and fixed LDA charge density implementations of the LDA+DMFT method. In order to compare our results obtained within the LMTO-ASA with the recent full-potential calculations of Andersson et $al.$[38], we have also carried out LDA and LDA+U calculations of Ce_2O_3. The LDA+U calculations have been performed using the same setup and U and J parameters than for LDA+DMFT, but using a Hartree-Fock approximation to the self-energy in the self-consistent calculations. The HF self-energy is obtained for an f occupancy, which can be different from the atomic one, therefore, in contrast to the HI case, in the LDA+U calculations we have used the actual (self-consistent) f-band occupancy in the expression for the double-counting correction.

Our results for the energy vs. lattice parameter curves are displayed in Fig 4. One may see that the localization of the Ce $4f$ electrons due to the strong local Coulomb correlations leads to a substantial increase in the lattice parameter. This is expected on a physical basis, since localization leads to a decreasing participation of these electrons to the cohesion of the solid. Our results for the equilibrium lattice parameter within the DMFT-nonSC, DMFT-SC and LDA+U methods are rather close to each other (3.79, 3.81 and 3.84 Å), and in reasonable agreement with the value 3.86 Å, obtained in Ref. [38] for a similar value of U, as well as with experiment (3.89 Å). The LDA lattice constant is much smaller (3.72 Å). The difference between the DMFT-nonSC and DMFT-SC for the equilibrium volume appears, somewhat surprisingly, to be rather small. The difference between the LDA+U and LDA+DMFT equilibrium volumes (i.e between Hartree-Fock and Hubbard-I approximations for the self-energy) stems possibly from the non-conserving nature of the HI approximation.
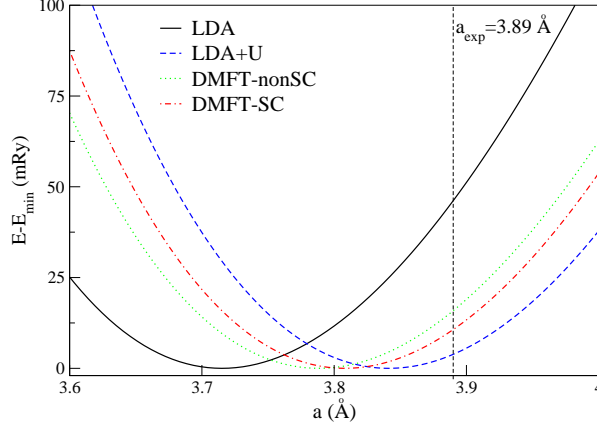
FIG. 4: (Color online). The total energy vs. lattice parameter dependence calculated within LDA (solid line), LDA+U (dashed line), DMFT-nonSC (dotted line) and DMFT-SC (dash-dotted line) approaches.The vertical dashed line indicates the experimental lattice parameter of Ce_2O_3

B. γ-Cerium
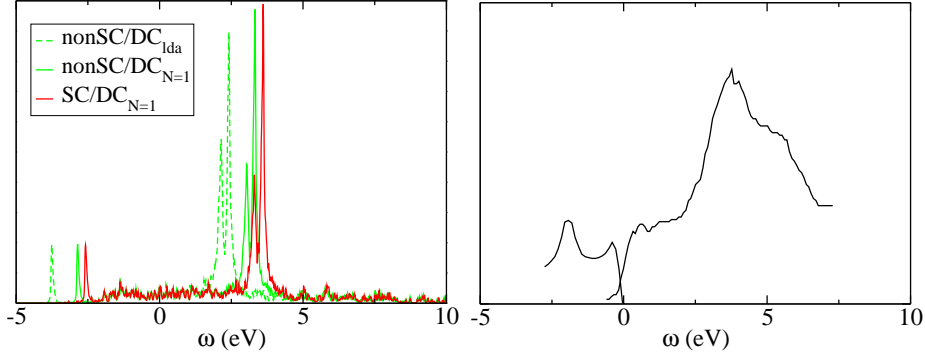

FIG. 5: (Color online). Spectral function for γ-Cerium within LDA+DMFT (Hubbard I) at T=0K with the self-consistent (SC) and non self-consistent (nonSC) schemes. In the first case, two ways of treating the double counting corrections are used: LDA number of electron and DMFT one (N=1 for the Hubbard I solver). Experimental spectrum (PES and BIS) of γ Cerium[45,46] are also represented.

As a second example, we have applied our DMFT-SC code to fcc-Cerium. This system has been thoroughly studied in the past in order to understand the α-γ transition[33], an isostructural volume collapse transition taking place as a function of temperature. Above the transition temperature T_c, in the large volume (γ-) phase, the f-electrons are localized, while the smaller volume in the α-phase below T_c leads to a more delocalized behavior of the f-electrons. Several model studies have been carried out to describe this transition[47,48,49]. More recently, it has also been studied in the framework of ab-initio calculations using LDA+DMFT[50,51,52,53,54,55,56,57]. However, these studies use the fixed charge density (non-SC) implementation of LDA+DMFT. Nevertheless, they were successful in describing the main aspects of the transition (spectra, and Kondo stabilization energy). The goal of our study is to evaluate the importance of self-consistency effects in LDA+DMFT calculations for Cerium. Since the most recent calculations[52,53,57] were done with the precise but time consuming Quantum Monte Carlo, it was not possible to test it. Another important goal is to study if a simple Hubbard I implementation of LDA+DMFT is able to describe correctly the γ phase of Cerium, in which electrons are more localized than in α Cerium.

Computations were done at the experimental volume of the γ phase for the spectra ($34.8Å^3$). 5p semicore
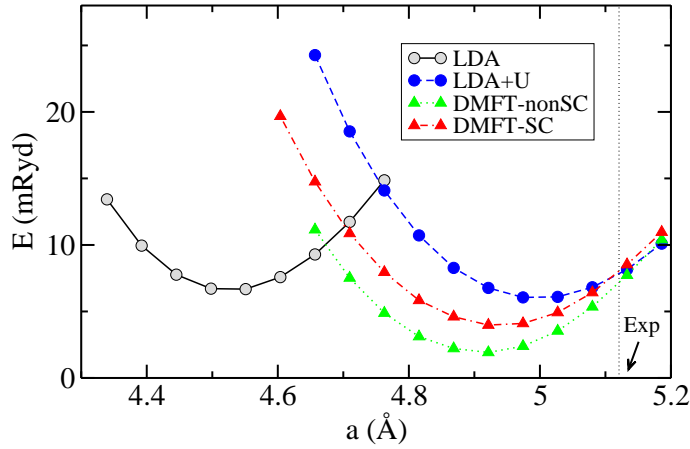
FIG. 6: (Color online). Total energy versus lattice parameter curves in LDA+DMFT (Hubbard I) for Cerium (shifts in energy between different curves are arbitrary).

states were taken into account thanks to an implementation of the LDA+DMFT self-consistency over density scheme with the multiple LMTO code[58]. Calculations with 5s states included do not show any change in the results. Valence states contain 5p 6s 6p 5d and 4f states. Calculations were done with 145 **k**-points in the irreducible Brillouin zone.

Figures 5 and 6 shows the spectral function and the total energy versus volume curves for fcc-Cerium for both the non-SC and the SC calculations. In accordance to calculations on Ce_2O_3, we use the 'atomic' number of electron computed in the Hubbard I solver to evaluate the double counting correction. It is more justified because of error compensation and, as we show below, the results for the lattice parameter at T=0 are consistent with LDA+U self-consistent calculations using the self-consistent number of electrons in the solid. For testing purposes, a non-SC calculations has also been done with the LDA number of electron in the double-counting correction.

Concerning the spectral function, we first see that all the calculations give the same qualitative physical pictures. The distance in energy between Hubbard bands is the same in all the calculations. The difference lies in the exact position of the Hubbard bands. The SC calculation gives the best agreement with experiment, the non-SC is shifted by 0.2 eV. The non-SC calculation with LDA double-counting is shifted by 1 eV with respect to the SC calculation. Table II gives the data necessary to understand these shifts, as explained before. We see that the effect of self-consistency itself is small in this case. The main error in the non-SC/DC_{LDA} comes from the double counting term, as expected. Note that non-SC and SC calculation lead to nearly the same number of electron. This can be partly attributed to the correlated character of the γ phase of Cerium: electrons are localized, so the number of electron is close to 1 (at least compared to an LDA calculation). Experimental spectra[45,46] of the gamma phase are also represented on figure 5. While the calculated position of the Hubbard bands is in good agreement with experiment, the width of the upper Hubbard band is not correctly described in our calculations. This is not surprising and is to be blamed on the use of a simplified Hubbard-I solver, which does not include lifetime effects. This means that Hubbard-I is only partly adequate to describe the high temperature γ-phase.

Figure 6 gives the total energy versus volume computed at T=0K. The main conclusion is that non-SC and SC DMFT calculations give the same minimum for the internal energy versus volume curves (see also table III). This value is not far from the value obtained in the LDA+U calculations in ASA (which is itself in good

	n_f	μ	$\langle H^f \rangle$	V_{DC}	$\langle \epsilon_f \rangle$
DMFT-nonSC/DC_{LDA}	1.06	0.23	0.45	3.94	-3.72
DMFT-nonSC/$DC_{N=1}$	1.04	0.26	0.45	2.99	-2.80
DMFT-SC/$DC_{N=1}$	1.04	0.10	0.57	2.99	-2.52

TABLE II: The number of electrons in DMFT, the chemical potential, the double counting contribution to the potential and the f level position in the DMFT-nonSC and DMFT-SC approaches for Cerium. Energies are in eV. The number of f-electrons in LDA is 1.16.

agreement with LDA+U calculations in PAW[59]). Note however that LDA+U can only account for correlation effects by introducing a spurious magnetic order, while DMFT is able to describe local moment formation and correlation effects in the paramagnetic phase. Effect of self-consistency appears to be fairly weak in the case of γ-cerium. One should also keep in mind that the ASA approximation does not describe correctly the bulk modulus in LDA. So the results concerning the energy versus volume curves should be taken only as trends. Moreover, direct comparison with experiment is difficult, because we have not computed the full free energy but only the internal energy[57].

Exp[60,61]	5.16
LDA+U/PAW[59]	5.05
LDA+U/ASA	5.00
DMFT SC/ASA	4.93
DMFT non-SC/ASA	4.91
LDA/PAW[59]	4.52
LDA/ASA	4.52

TABLE III: Lattice parameter (in Å) of γ Cerium according to experimental data, PAW calculations and our calculations.

The calculations where 6p states are not taken into account leads to an underestimation of the lattice parameter (4.80 Å instead of 4.93 Å). This is in accordance to the underestimation of the lattice parameter in LDA when 6p states are neglected (4.44 Å instead of 4.52 Å)

Our conclusion regarding γ-cerium is that spectra and energy are reasonably described with a fixed (LDA, non-SC) charge density approximation. However, it is mandatory to use a self-consistent implementation to obtain more accurate results.

IV. CONCLUSION

In conclusion, we have devised a simple and efficient implementation of the fully self-consistent LDA+DMFT method in the LMTO basis set. The charge density is calculated from moments involving the LDA+DMFT momentum-distribution matrix and the KS hamiltonian. We have also obtained accurate formulas for computing the total energy by handling high-frequency tails of the Green's function and self-energy in an appropriate manner.

We have computed the local and **k**-resolved spectral functions of cerium sesquioxide Ce_2O_3 by means of the fully self-consistent LDA+DMFT technique in conjunction with the Hubbard-I approximation for the DMFT self-energy. We have shown that the charge-density self-consistency affects the spectral properties of Ce_2O_3 substantially, causing a shift of the lower Hubbard band by approximately 1 eV and a corresponding decrease in the value of the band gap in comparison with DMFT calculations with fixed LDA charge density; This effect considerably improves the agreement with experiment in comparison to a non-self consistent calculation using the LDA charge density. We have identified the main cause of these modifications, which is due to a significant change in the effective KS band structure, computed with LDA+DMFT charge density, as compared to the LDA band structure.

Finally, we have obtained the total energy and equilibrium volume of γ-Ce within the fixed (LDA) charge and fully self-consistent LDA+DMFT schemes. The effects of the self-consistency over the charge density are less important for γ-Ce than for the oxide: self-consistency induces in this case a change of 1% on the ground-state volume, and affects the spectral function by shifts of a fraction of an electron-Volt only.

ACKNOWLEDGMENTS

---

[1] W. Kohn, Rev. Mod. Phys. **71**, 1253 (1999).

[2] R. O. Jones and O. Gunnarsson, Rev. Mod. Phys. **61**, 689 (1989).

[3] A. Georges, G. Kotliar, W. Krauth, and M. J. Rozenberg, Rev. Mod. Phys. **68**, 13 (1996).

[4] V. I. Anisimov, A. I. Poteryaev, M. A. Korotin, A. O. Anokhin, and G. Kotliar, J. Phys.: Condens. Matter **9**, 7359 (1997).

[5] A. I. Lichtenstein and M. I. Katsnelson, Phys. Rev. B **57**, 6884 (1998).

[6] S. Biermann, *in Encyclopedia of Materials: Science and Technology* (Elsevier Ltd, 2006), available online at: www.sciencedirect.com.

[7] A. Georges, in *Lectures on the physics of highly correlated electron systems VIII*, edited by A. Avella and F. Mancini (American Institute of Physics, 2004), cond-mat/0403123.

[8] G. Kotliar, S. Y. Savrasov, K. Haule, V. S. Oudovenko, O. Parcollet, and C. A. Marianetti, Rev. Mod. Phys. **78**, 865 (2006).

[9] K. Held, I. A. Nekrasov, G. Keller, V. Eyert, A. K. M. N. Blümer, R. T. Scalettar, T. Pruschke, V. I. Anisimov, and D. Vollhardt, *in Quantum Simulations of Complex Many-Body Systems: From Theory to Algorithms (NIC Series Vol. 10)* (2002).

[10] S. Y. Savrasov and G. Kotliar, Phys. Rev. B **69**, 245101 (2004).

[11] J. Minár, L. Chioncel, A. Perlov, H. Ebert, M. I. Katsnelson, and A. I. Lichtenstein, Phys. Rev. B **72**, 045125 (2005).

[12] F. Lechermann, A. Georges, A. Poteryaev, S. Biermann, M. Posternak, A. Yamasaki, and O. K. Andersen, Phys. Rev. B **74**, 125120 (2006).

[13] V. I. Anisimov, A. V. Kozhevnikov, M. A. Korotin, A. V. Lukoyanov, and D. A. Khafizullin, J. Phys.: Condens. Matter **19**, 106206 (2007).

[14] P. Lambin and J. P. Vigneron, Phys. Rev. B **29**, 3430 (1984).

[15] J. Hubbard, Proc. Roy. Soc. (London) **A 276**, 238 (1963).

[16] N. V. Skorodumova, R. Ahuja, S. I. Simak, I. A. Abrikosov, B. Johansson, and B. I. Lundqvist, Phys. Rev. B **64**, 115108 (2001).

[17] E. Pavarini, S. Biermann, A. Poteryaev, A. I. Lichtenstein, A. Georges, and O. K. Andersen, Phys. Rev. Lett. **92**, 176403 (2004).

[18] V. I. Anisimov, D. E. Kondakov, A. V. Kozhevnikov, I. A. Nekrasov, Z. V. Pchelkina, J. W. Allen, S.-K. Mo, H.-D. Kim, P. Metcalf, S. Suga, et al., Phys. Rev. B **71**, 125119 (2005).

[19] O. K. Andersen, Phys. Rev. B **12**, 3060 (1975).

[20] H. L. Skriver, *The LMTO method* (Springer, Berlin, 1984).

[21] O. K. Andersen, T. Saha-Dasgupta, R. W. Tank, C. Arcangeli, O. Jepsen, and G. Krier, in *Electronic Structure and Physical Properties of Solids. The Use of the LMTO Method, Lectures of a Workshop Held at Mont Saint Odile, France, October 2-5, 1998. Edited by H. Dreyssé, Lecture Notes in Physics, vol. 535, p.3* (2000), p. 3.

[22] O. K. Andersen, O. Jepsen, and M. Sob, *in Electronic Band Structure and Its Applications* (Springer-Verlag, Berlin, 1986).

[23] P. Löwdin, J. Chem. Phys. **18**, 365 (1950).

[24] W. R. L. Lambrecht and O. K. Andersen, Phys. Rev. B **34**, 2439 (1986).

[25] G. Kotliar and S. Y. Savrasov, *Dynamical Mean Field Theory, Model Hamiltonians and First Principles Electronic Structure Calculations* (In "New Theoretical Approaches to Strongly Correlated Systems, A.M. Tsvelik Ed., Kluwer Academic Publishers, 2001), proc. of the Nato Advanced Study Institute on New Theoretical Approaches to Strongly Correlated Systems, Cambridge, UK, 1999; preprint cond-mat/0208241.

[26] G. Kotliar, S. Y. Savrasov, K. Haule, V. S. Oudovenko, O. Parcollet, and C. A. Marianetti, Rev. Mod. Phys. **78**, 865 (2006).

[27] J. M. Luttinger and J. C. Ward, Phys. Rev. **118**, 1417 (1960).

[28] J. J. Deisz, D. W. Hess, and J. W. Serene, *in Recent Progress In Many Body Theories, vol. 4* (Plenum, New York, 1995), preprint cond-mat/9411026.

[29] J. J. Deisz, D. W. Hess, and J. W. Serene, Phys. Rev. B **66**, 014539 (2002).

[30] L. V. Pourovskii, M. I. Katsnelson, and A. I. Lichtenstein, Phys. Rev. B **72**, 115106 (2005).

[31] V. I. Anisimov, F. Aryasetiawan, and A. I. Lichtenstein, J. Phys. Condensed Matter **9**, 767 (1997).

[32] A. I. Lichtenstein, M. I. Katsnelson, and G. Kotliar, Phys. Rev. Lett. **87**, 067205 (2001).

[33] D. G. Koskimaki and K. A. Gschneidner, *in Handbook on the Physics and Chemistry of Rare Earths* (North-Holland, Amsterdam, 1978).

[34] A. K. McMahan, C. Huscroft, R. T. Scalettar, and E. L. Pollock, J. Comput.-Aided Mater. Des. **5**, 131 (1998).

[35] L. Petit, A. Svane, Z. Szotek, and W. M. Temmerman, Topics in Applied Physics **106**, 331 (2007).

[36] S. Fabris, S. de Gironcoli, S. Baroni, G. Vicario, and G. Balducci, Phys. Rev. B **71**, 041102(R) (2005).

[37] N. Singh, S. M. Saini, T. Nautiyal, and S. Auluck, J. Applied Phys. **100**, 083525 (2006).

[38] D. A. Andersson, S. I. Simak, B. Johansson, I. A. Abrikosov, and N. V.Skorodumova, Phys. Rev. B **75**, 035109 (2007).

[39] C. Loschen, J. Carrasco, K. M. Neyman, and F. Illas, Phys. Rev. B **75**, 035115 (2007).

[40] J. L. F. DaSilva, M. V. Ganduglia-Pirovano, J. Sauer, V. Bayer, and G. Kresse, Phys. Rev. B **75**, 045121 (2007).

[41] R. W. G. Wyckoff, *in 2nd Edition, Crystal Structures, Vol.2* (1967), p. 1.

[42] V. I. Anisimov and O. Gunnarsson, Phys. Rev. B **43**, 7570 (1991).

[43] J. F. Herbst, R. E. Watson, and J. W. Wilkins, Phys. Rev. B **17**, 3089 (1978).

[44] A. V. Golubkov, A. V. Prokof'ev, and A. I. Shelykh, Phys. Solid State **37**, 1028 (1995).

[45] E. Wuilloud, H. R. Moser, W.-D. Schneider, and Y. Baer, Phys. Rev. B **28**, 7354 (1983).

[46] D. Wieliczka, J. H. Weaver, D. W. Lynch, and C. G. Olson, Phys. Rev. B **26**, 7056 (1982).

[47] B. Johansson, Phil. Mag. **30**, 469 (1974).

[48] M. Lavagna, C. Lacroix, and M. Cyrot, Phys. Lett. A **90**, 210 (1982).

[49] L. Z. Liu, J. W. Allen, O. Gunnarsson, N. E. Christensen, and O. K. Andersen, Phys. Rev. B **45**, 8934 (1992).

[50] J. Lægsgaard and A. Svane, Phys. Rev. B **59**, 3450 (1999).

[51] M. B. Zölfl, I. A. Nekrasov, T. Pruschke, V. I. Anisimov, and J. Keller, Phys. Rev. Lett. **87**, 276403 (2001).

[52] K. Held, A. K. McMahan, and R. T. Scalettar, Phys. Rev. Lett. **87**, 276404 (2001).

[53] A. K. McMahan, K. Held, and R. T. Scalettar, Phys. Rev. B **67**, 075108 (2003).

[54] A. K. McMahan, Phys. Rev. B **72**, 115125 (2005).

[55] K. Haule, V. Oudovenko, S. Y. Savrasov, and G. Kotliar, Phys. Rev. Lett. **94**, 036401 (2005).

[56] O. Sakai, Y. Shimizu, and Y. Kaneta, J. Phys. Soc. Jpn. **74**, 2517 (2005).

[57] B. Amadon, S. Biermann, A. Georges, and F. Aryasetiawan, Phys. Rev. Lett. **96**, 066402 (2006).

[58] F. Aryasetiawan and O. Gunnarsson, Phys. Rev. B **49**, 7219 (1994).

[59] B. Amadon, F. Jollet, and M. Torrent, unpublished results (2007).

[60] I.-K. Jeong, T. W. Darling, M. J. Graf, T. Proffen, R. H. Heffner, Y. Lee, T. Vogt, and J. D. Jorgensen, Phys. Rev. Lett. **92**, 105702 (2004).

[61] J. S. Olsen, L. Gerward, U. Benedict, and J. P. Itie, Physica B **133**, 129 (1985).

[62] One may notice that in Fig. 3 the chemical potential is pinned little bit above the bottom of the conduction band. This is actually a drawback of the Hubbard-I approximation, in which the insulating plateau on the $n(\mu)$ curve is not exactly at a commensurate filling (due to the non-conserving nature of the Hubbard-I approximation). This is a very small effect, however (of order of 0.01% of the total electronic charge), therefore producing a negligible change in the total charge density.